Coarsening dynamics of the one-dimensional Cahn-Hilliard model

M. Argentina,[1,2] M. G. Clerc, R. Rojas,[1,3,*] and E. Tirapegui[1,3]
[1]*Departamento de Física, Facultad de Ciencias Físicas y Matemáticas, Universidad de Chile, Casilla 487-3, Santiago, Chile*
[2]*DAMTP, Silver Street, CB3 9EW Cambridge, United Kingdom*
[3]*Centro de Física No Lineal y Sistemas Complejos de Santiago, Casilla 27122 Correo 27, Santiago, Chile*
(Received 14 July 2004; published 18 April 2005)

The dynamics of one-dimensional Cahn-Hilliard model is studied. The stationary and particle-type solutions, the bubbles, are perused as a function of initial conditions, boundary conditions, and system size. We characterize the bubble solutions which are involved in the coarsening dynamics and establish the bifurcation scenarios of the system. A set of ordinary differential equation permits us to describe the coarsening dynamics in very good agreement with numerical simulations. We also compare these dynamics with the bubble dynamics deduced from the classical kink interaction computation where our model seems to be more appropriated. In the case of two bubbles, we deduce analytical expressions for the bubble's position and the bubble's width. Besides, a simple description of the ulterior dynamics is presented.

DOI: 10.1103/PhysRevE.71.046210 PACS number(s): 05.45.−a, 05.70.Np, 64.75.+g

I. INTRODUCTION

Interfacial instabilities and pattern formation have stimulated a great amount of studies during the last decades [1]. In most cases, the interface is a moving boundary separating two different domains. For example, in crystal growth, rich morphological instabilities may arise from destabilization of the solidification front, see Ref. [2] for a specific review and also Ref. [3] more generally. In the two-dimensional extended system, the domains dynamics are described by interface propagation. Its dynamics can be treated as the evolution of unidimensional curves [4]; usually, it is characterized by a nonlocal equation in space [5], hence their study is difficult in general. When an almost flat interface undergoes an instability, its dynamics become local, as the interface exhibits slow variation in space (see, for example, Ref. [6]). As a consequence, one can take into account the field $P(t,x)$, which describes the slowly varying interface position parametrized by the space variable x at the instant t. Henceforth, for the sake of simplicity, we consider that the interface is initially flat. If the system under study is isotropic, the interface dynamics must be invariant under spatial translation, since a solid translation of the interface ($P \to P+P_o$) does not affect the interface dynamics. Thus the interface position must satisfy an equation of the form

$$\partial_t P(x,t) = F(\partial_x^n P, n = 1, \ldots). \tag{1}$$

The isotropic hypothesis also provides a reflection symmetry with respect to the direction of the flat interface (tangential direction, $x \to -x$), then the interface perturbations are described asymptotically by

$$\partial_t P(x,t) = \varepsilon P_{xx} \pm P_x^2, \tag{2}$$

where the first term of the right hand side stands for a diffusive effect, if the control parameter ε is positive. The last term represents nonlinear advective effects. The dynamics exhibited by Eq. (2) is characterized by a spreading of the perturbations. When the perturbed interface is almost flat, the dynamics are governed by the heat equation, since the nonlinear term of system (2) is not dominant. Since the position of the interface is arbitrary due to the translational symmetry ($P \to P+P_o$), the position $[P(x,t)]$ is not a standard order parameter, because it is not small in general. Instead, it is desirable to consider the spatial gradient of the interface position ($u=P_x$), which is a good order parameter in the classical sense, $u \ll 1$, and satisfies the Burgers equation [7].

When $\varepsilon > 0$, the above model describes the evolution of stable perturbations of a flat interface in an anisotropic medium. This flat interface exhibits a spatial instability when ε is negative. In the case of small ε (positive or negative), it is necessary to take into account higher derivatives and the interface is described asymptotically by the new system

$$\partial_t P(x,t) = \varepsilon P_{xx} \pm P_x^2 - P_{xxxx}, \tag{3}$$

which is the well-known Kuramoto-Sivashinsky equation [8,9]. It has been derived by Sivashinsky to describe the diffusive instabilities of planar flame fronts [9,10] and by Kuramoto within the framework of phase dynamics in reaction-diffusion systems [8].

The general above picture is modified when one considers extra symmetries, in which case the interface dynamics is not described by Eq. (2). For example, this situation arises for an interface that separates symmetrical domains with energetically equivalent states, like those observed in a magnetic domain [11] or in the Ising wall model elegantly exhibited in liquid crystals [12,13]. In all these cases, the interfaces connect two symmetrical states and an extra symmetry appears ($P \to -P$) that prohibits the nonlinear advective term in Eq. (2). The interface dynamics becomes described by

*Permanent address: Institut Non Linéaire de Nice, UMR 6618 CNRS-UNSA, 1361 Route des Lucioles, F-06560 Valbonne, France.

$$\partial_t P(x,t) = \varepsilon P_{xx} + a P_x^2 P_{xx}, \tag{4}$$

where the last term represents the effect of a nonlinear diffusion ($a>0$) or antidiffusion ($a<0$). The above model is characterized by diffusive dynamics ($\varepsilon>0$), that is, the interface tends to reduce its local curvature. This model is also a continuity equation, which expresses the conservation of the area under the curve $P(x,t)$. This property is a consequence of the fact that if the interface moves over one domain then it also moves over the other domain, since both states are energetically equivalent.

In the case of small (either positive or negative) ε, the interface is described asymptotically by

$$\partial_t P(x,t) = \varepsilon P_{xx} + 3P_x^2 P_{xx} - P_{xxxx}, \tag{5}$$

where the sign of the last term has been chosen in order to saturate linearly the spatial instability for large wave number.

We remark that the above model is also a continuity equation. It is variational, since one can write

$$\partial_t P = -\frac{\delta F}{\delta P},$$

$$F[P] = \int dx \left\{ \varepsilon \frac{P_x^2}{2} + \frac{P_x^4}{4} + \frac{P_{xx}^2}{2} \right\}, \tag{6}$$

where the *free energy* F depends only on the derivatives of $P(x,t)$. Introducing the variable $u \equiv P_x$ which is a standard order parameter ($u \ll 1$), the above equation is transformed into the Cahn-Hilliard equation [14]

$$\partial_t u = \partial_{xx}(\varepsilon u + u^3 - u_{xx}) = \partial_{xx} \frac{\delta F[u]}{\delta u(x)}, \tag{7}$$

which is a continuity equation with the Lyapunov functional [15],

$$F[u] \equiv \int dy \left[\varepsilon \frac{u^2}{2} + \frac{u^4}{4} + \frac{u_y^2}{2} \right].$$

The Cahn-Hilliard equation has been derived in order to describe the phase separation dynamics in a conservative system, such as binary alloys [16], binary liquids [17], glasses [18], and polymer solutions [19] to mention a few. Note that this model also describes the zigzag instability undergone by straight rolls in two-dimensional extended systems like Rayleigh-Bénard convection [20] or electroconvection [21] in fluid systems, and it has been extensively studied over the last decades [1]. A similar zigzag instability affecting anisotropic interfaces has recently aroused considerable interest in different fields [22,23], for example, in gas discharge system [24], rifts in spreading wax layer [25], Ising wall in smectic, nematic, cholesteric liquid crystals, and liquid crystal electroconvection [13,22,23,26].

A successful strategy to study partial differential equations (PDEs) consists in studying particle or defectlike type solutions [1,27–31,33] which have the property of being localized in space. If, after some transient, a solution consisting of a certain number of these localized structures is established, one can describe the ulterior dynamics of the system through the evolution of these solutions due to their mutual interactions, and this evolution turns out to be determined in many cases by ordinary differential equations (ODEs) [1,27]. The previous scenario is based on the fact that particle type solutions have Goldstone modes. This means that they have a neutral mode related to a continuous invariance, for example the spatial translation. Hence the evolution of these solutions, when they are sufficiently diluted (spaced apart), is obtained through the Goldstone modes. Consequently, the temporal evolution associated to the mutual influence of localized structures exhibits slow dynamics.

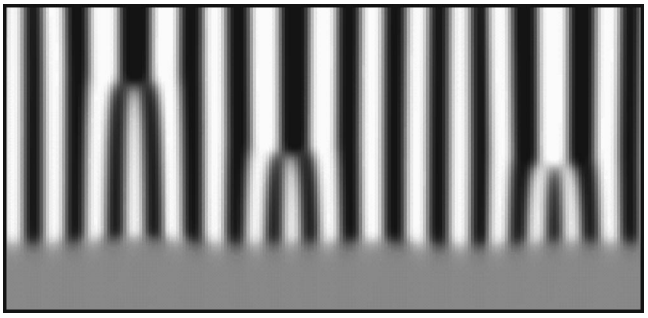

FIG. 1. Spatiotemporal evolution of the Cahn-Hilliard model in the spinodal decomposition regime. Time is running up (800 time units), system size $L=200$, $\epsilon=-0.5$. White color represents -0.6 and the black one 0.6.

These interactions are typically exponential with respect to the distance between the defects [33]. The process of the appearance and the ulterior evolution of these defects solutions is well known as coarsening dynamics. Then we see that in this way we can have a simplified description with ODE of the physical phenomenons occurring in the system [1,27–30,33], and in particular in the Cahn-Hilliard equation [32–35].

This paper is organized as follows. The dynamical description and characterization of stationary solutions of the Cahn-Hilliard equation is addressed in Sec. II. A great amount of work has been devoted to the study of the stationary solutions [36–40] and their bifurcations. We propose here a unified description for stationary solutions and their bifurcations, which also reproduces these former works. Our approach allows us to have a qualitative and quantitative understanding of the bifurcations scenarios. The dynamics of a diluted gas of bubbles which characterize the coarsening dynamics is addressed in Sec. III. We also compare our results with previous works [32–35]. The interaction of two bubbles in a periodic domain is analyzed in great detail. We summarize our results and conclude in the last section.

II. DESCRIPTION STATIONARY SOLUTIONS AND THEIR LINEAR STABILITY

When the diffusion coefficient ε of the Cahn-Hilliard model is positive, the perturbation of the flat solution $[u(x,t)=P_x=0]$ is ruled out by the heat equation and the modes of largest wave numbers decay faster than the smallest ones.

In the case of negative ε, the flat solution is spatially unstable. By perturbing initially this solution with noise and

following the ulterior evolution, one can observe initially the appearance of a periodic pattern with a well-defined wave number weakly modulated: this is trivially deduced from the linear study around the flat solution. Successively, the smallest bumps merge together forming new larger bumps (see Fig. 1): this process is well known as spinodal descomposition [41]. A recent experimental study of an interface between two convective states in electroconvection of liquid crystals showed that, in the coarsening regime, the average separation between the bubbles increases logarithmically in time [13], in agreement with the theoretical prediction [32,42].

In the next sections, we will present an analytical description of the stationary solutions, bifurcation scenarios, and coarsening dynamics observed in the one-dimensional Cahn-Hilliard equation.

A. Stationary bubble solutions

The stationary solutions of the one-dimensional Cahn-Hilliard equation has been studied in great detail by Novick-Cohen and co-workers [36,37,39,40]. We propose in this section an alternative study of the stationary inhomogeneous solution and assess the behavior of these solutions in the large and small domain size. The existence of (multi)bubble solution is related to the bifurcations of the homogeneous solutions [39]. We refer to bubble solutions as a pair of kink-antikink profile. From this scheme, stability of the (multi)bubble solution will be found, using a different approach than the former works [32–35]. Since the Cahn-Hilliard model possesses a Lyapunov functional, the knowledge of its stationary solution permits us to give a qualitative picture of the dynamics. It is in this spirit that the coarsening process is understood as a flow in the PDE phase space that successively passes near the unstable stationary solution containing n bubbles, $n-1$, until the system is relaxed to the global minimum of the Lyapunov functional (a bubble in periodic boundary condition or a kink with zero flux boundary condition) [34,35]. From the analysis, it is deduced that the coarsening dynamics is exponentially slow [43].

By appropriate scalings, the bifurcation parameter ε can be set equal to -1 when it is negative, and Eq. (7) is transformed into

$$\partial_t u = \partial_{xx}(-u + u^3 - \partial_{xx}u), \tag{8}$$

with periodic boundary conditions or Neumann type boundary conditions, i.e., null flux at the boundary. The area under the $u(x,t)$ field is conserved during the time evolution, $S = \int_0^L u(x,t)dx$. Stationary solutions are therefore functions of the area S and the system size, which can be finite or infinite; they obey the equation

$$-u + u^3 - \partial_{xx}u - \lambda = 0,$$

where λ is an integration constant and is *a priori* arbitrary. Due to the symmetry $\lambda \to -\lambda$ and $u \to -u$, we will suppose without loss of generality that $\lambda > 0$. The above Newton type equation is integrated into

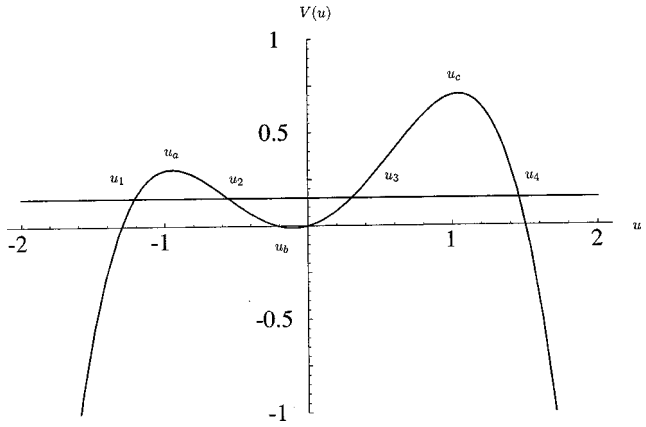

FIG. 2. Potential $V(u)$ as a function of u, for $\lambda = 0.2$.

$$V(u) + (\partial_x u)^2 = E, \tag{9}$$

where the potential energy is $V(u) = 2\lambda u + u^2 - u^4/2$ (cf. Fig. 2).

B. Homogeneous solutions and their stability

The potential $V(u)$ has three extrema if $\lambda^2 < \lambda_c^2$, $\lambda_c \equiv 2/(3\sqrt{3})$. We will note them $u_a \leqslant u_b \leqslant u_c$ and they are given by

$$u_a = -2\sqrt{\frac{1}{3}}\sin\left(\frac{1}{3}\arctan\sqrt{\frac{4}{27\lambda^2}-1} + \frac{\pi}{6}\right),$$

$$u_b = 2\sqrt{\frac{1}{3}}\sin\left(\frac{1}{3}\arctan\sqrt{\frac{4}{27\lambda^2}-1} - \frac{\pi}{6}\right),$$

$$u_c = 2\sqrt{\frac{1}{3}}\cos\left(\frac{1}{3}\arctan\sqrt{\frac{4}{27\lambda^2}-1}\right).$$

Note that $\frac{1}{3} < u_{a,c}^2 < 1$, and $-1/\sqrt{3} < u_b < 0$. Let us investigate the linear stability of a homogeneous solution u_0 with respect to an inhomogeneous spatial perturbation. This latter, that we name $v (v \equiv u - u_0)$, obeys

$$\partial_t v = \partial_{xx}[v(-1 + 3u_0^2) - \partial_{xx}v].$$

In Fourier space, this relation becomes

$$\partial_t v_p = p^2[(1 - 3u_0^2) - p^2]v_p,$$

where v_p is the amplitude of a harmonic perturbation with a spatial frequency p. Therefore, if $1 - 3u_0^2 \leqslant 0$, the solution is stable whatever the perturbing wave number is. Since u_a and u_c are bigger in absolute value than $1/\sqrt{3}$, the potential maxima are stable. The stability of the minimum u_b depends on the domain size. If the domain is infinite, then p can be as small as possible and the solution u_b will be unstable toward large wavelength perturbations. It is related to the classical spinodal decomposition, for which the Cahn-Hilliard model has been historically derived [14]. If the domain is finite, the quantified wave number p may be large enough and such that u_b remains stable. For larger system size, the smallest wave

number $2\pi/L$ renders this solution unstable when $(1-3u_0^2)=p^2$; in terms of the area S ($S=u_bL$) and the system size L, this bifurcation point is

$$\begin{cases} L_1^B = \sqrt{3S^2+4\pi^2}, \\ \lambda_1^B = -2S\dfrac{S^2+2\pi}{(3S^2+4\pi^2)^{3/2}}. \end{cases} \tag{10}$$

This instability corresponds to a saddle node bifurcation under O(2) symmetry due to the space translation symmetry. In fact, there is a bifurcation occurring for each Fourier mode which becomes unstable with a spatial frequency $2n\pi/L$, this occurs when

$$\begin{cases} L_n^B = \sqrt{3S^2+4n^2\pi^2}, \\ \lambda_n^B = -2S\dfrac{S^2+2n^2\pi^2}{(3S^2+4n^2\pi^2)^{3/2}}. \end{cases} \tag{11}$$

This means that the homogeneous solutions have n positive eigenvalues in the range $\lambda_{n+1}^B<\lambda<\lambda_n^B$. At the nth bifurcation point, i.e., for $L=L_n$, the positive eigenvalues are

$$\sigma_i = \left(\frac{4i\pi^2}{3S^2+4n^2\pi^2}\right)^2 (n^2-i^2), \quad \text{for } i=1\cdots n.$$

Consequently, in the bifurcation diagram, branches of new solutions are expected to cross the homogeneous branch solution at bifurcation points. These new solutions must be spatially inhomogeneous, since we have already explored all the trivial solutions.

C. Inhomogeneous solutions and bubbles

In this section we determine the inhomogeneous solutions that take the form of kinks, solutions that connect at $\pm\infty$ two different stationary states when the domain is large enough. The potential $V(u)$ must have at least one minimum, and this is insured, as it results from the above analysis, if $\lambda^2<\lambda_c^2$. With such an assumption, one can write

$$(\partial_x u)^2 = \frac{(u-u_1)(u-u_2)(u-u_3)(u-u_4)}{2}, \tag{12}$$

where the roots of $\partial_x u$ are real and expressed as function of λ and E, and we assume that $u_1\leqslant u_2\leqslant u_3\leqslant u_4$ as pictured in Fig. 2. Equation (12) can be directly integrated and we obtain the bubble solution

$$U(x) = u_4 - \frac{(u_4-u_2)(u_4-u_3)}{(u_4-u_2)-(u_3-u_2)\mathrm{sn}(y|m)^2} \tag{13}$$

with $y=(1/2\sqrt{2})\sqrt{(u_3-u_1)(u_4-u_2)}(x-x_o)$ and $m=(u_4-u_1)\times(u_3-u_2)/[(u_3-u_1)(u_4-u_2)]$. The function $\mathrm{sn}(\phi|n)$ is a Jacobi elliptic function [44]. This solution is well known [36,37] and has as period

$$L = \frac{4\sqrt{2}}{\sqrt{(u_4-u_2)(u_3-u_1)}}\mathrm{K}(m), \tag{14}$$

where the function $\mathrm{K}(m)$ is the complete elliptic integral of the first kind. The period logarithmically diverges when the solution tends to be a homoclinic trajectory, i.e., for $u_1\to u_2$ implying $m\to 1$. From the solution (13) one can explicitly obtain the area S

$$S = \frac{4\sqrt{2}[u_1\mathrm{K}(m)+(u_2-u_1)\Pi(n_1,m_1)]}{\sqrt{(u_3-u_1)(u_4-u_2)}}, \tag{15}$$

where $n_1=(u_3-u_2)/(u_3-u_1)$ and $m_1=(u_2-u_3)(u_4-u_1)/(u_1-u_3)(u_2-u_4)$. $\Pi(n_1,m_1)$ is the elliptic integral of the third kind.

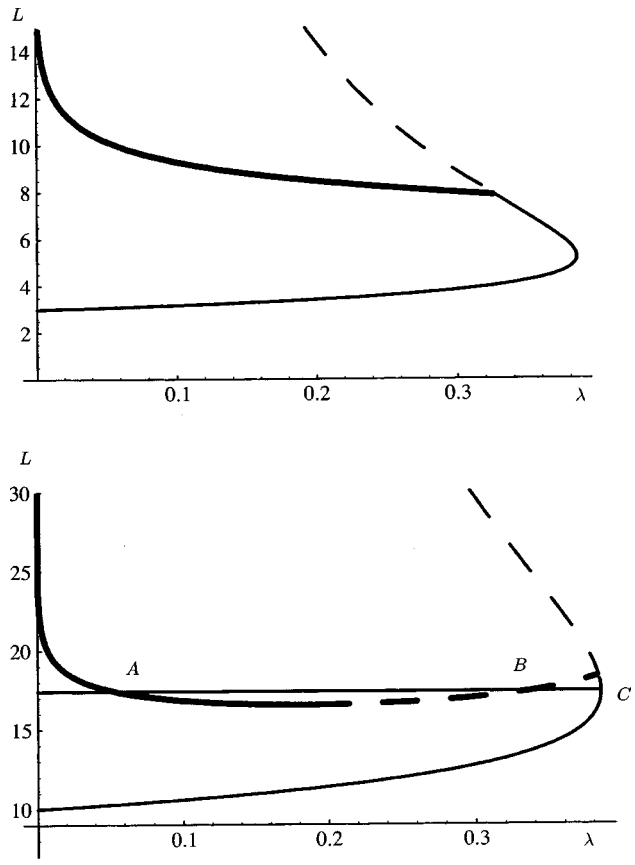

FIG. 3. Period of the solutions that have a fixed area $S=-3$ (a) and $S=-30$ (b). The thin line represents the period of homogeneous solutions; the lowest curve represents the period of u_b and the highest one, the period of u_a. The thick line represents the period of the bubble solution. The dashed (respectively solid) line represents unstable (respectively stable) solutions. Stationary solutions A (stable bubble solution), B (unstable bubble solution), and C (stable homogeneous solution) are found by the intersection of these curves with the line $L=17.5$.

D. Construction of the solutions

To compute the explicit solution of the problem, one needs to fix the area S and the system size L, which are conserved during temporal evolution. Fixing the two last quantities permits the inversion of the relations (14) and (15) and gives a value for λ and E. These values determine the dynamical system (9), and we can now construct its solutions. An example of numerical inversion is shown in Fig. 3

Similar bifurcation diagrams have been derived numerically [45]. From Fig. 3(b), it is seen that if the area S is large

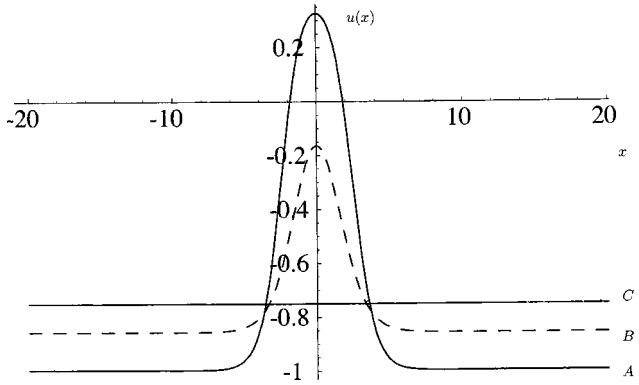

FIG. 4. Plot of the field u of the bubble A in the thick line, the nucleation solution B in the thick dashed line, and the homogeneous solution C ($L=17.5$, and $S=-30$).

enough in absolute value, the system is bistable for small domain size. In that case, it has as stationary solution the homogeneous solution and an inhomogeneous one that represents the bubble solution. Note that if the system size is too small, there is no bubble solution. At $\lambda=\lambda_1$, there is a saddle bifurcation under O(2) symmetry (the new solution breaks the translation invariance) occurring at the branching point of the two families of solutions, whose normal form is [37], for the supercritical bifurcation,

$$\frac{dA}{dt}=\mu A-|A|^2A.$$

The point of bifurcation is related to the bifurcation of the u_b solution, derived in the previous section,

$$\lambda_1^B=-2S\frac{2\pi^2+S^2}{(4\pi^2+3S^2)^{3/2}}.$$

In the case of large area (cf. Fig. 4), bistability occurs between the bubble solution A and the homogeneous solution C. Since the system is potential, an extremum solution must exist. It is related to a nucleation solution whose codimension-1 stable manifold is the nucleation barrier (manifold) separating two stable solutions; it is a separatrix in the functional space. Mathematical properties of this nucleation manifold has been studied in Ref. [46]. This feature will be explained in detail in the text, where the small domain size approximation is performed.

In the two following subsections, we compute analytically the branches of the bubbles solutions in two limits: for large and small domain size.

E. Large domain size ($L\to\infty$)

For the sake of simplicity, we will work with the variable u_a, defined from λ, such that $\lambda=-u_a+u_a^3$. The solution with an infinite period ($L\to\infty$) is obtained taking the limit $u_1\to u_2\equiv u_a$, and we obtain

$$U_h(x)=u_a+\frac{2(3u_a^2-1)}{-2u_a+\sqrt{2(1-u_a^2)}\cosh[(x-x_0)\sqrt{3u_a^2-1}]}. \tag{16}$$

This is a known solution and has been derived in Refs. [15,36]. The above expression can be rewritten in the following form:

$$U_h(x)=u_a+\sqrt{\frac{3u_a^2-1}{2}}\left\{\tanh\left[\frac{\sqrt{3u_a^2-1}}{2}\left(x-x_0+\frac{\delta}{2}\right)\right]-\tanh\left[\frac{\sqrt{3u_a^2-1}}{2}\left(x-x_0-\frac{\delta}{2}\right)\right]\right\}, \tag{17}$$

where $\delta=2/\sqrt{3u_a^2-1}\arccos h[-2u_a/\sqrt{2(1-u_a^2)}]$. When L is large enough, the function $\tanh(x)$ converges exponentially to a constant and it is possible to approximate the exact solution (13) with Eq. (17), since the error is exponentially small. The computation of this correction is straightforward, but needs a lot of algebra (details of the calculation will be omitted), and gives

$$32\frac{(1-3u_a^2)^3}{1-u_a^2}e^{-2L\sqrt{3u_a^2-1}}.$$

If $1-3u_a^2$ is different from 0, the large domain size approximation captures very well the solution, since the error is exponentially small ($e^{-2L\sqrt{1-3u_a^2}}$). When $1-3u_a^2$ approaches zero, the solution is also well captured for small domain size, but the error becomes algebraic [$(1-3u_a^2)^3$]. Note that $u_a=-1/\sqrt{3}$ corresponds to $\lambda=\lambda_c$.

In the large domain limit, we evaluate the bubble's area S, by integrating relation (17) in the whole finite domain: this leads to

$$S=u_aL+2\sqrt{2}\ln\left(\frac{\cosh\left[\frac{\sqrt{3u_a^2-1}}{4}(\delta+L)\right]}{\cosh\left[\frac{\sqrt{3u_a^2-1}}{4}(\delta-L)\right]}\right).$$

This expression can be simplified when the system size is large enough:

$$S=u_aL+2\sqrt{2}\,\mathrm{arccosh}\left(\frac{-\sqrt{2}u_a}{\sqrt{1-u_a^2}}\right),$$

and we obtain the relation between the approximation of the period of the solution as a function of its area and u_a:

$$L^A=\frac{1}{u_a}\left[S-2\sqrt{2}\,\mathrm{arccosh}\left(\frac{-\sqrt{2}u_a}{\sqrt{1-u_a^2}}\right)\right]. \tag{18}$$

Hence the solutions defined with u_a and their branches can be found easily by a simple numerical inversion of the above implicit equation. This relation is compared with the numerical computation presented in Fig. 5, where this large domain approximation matches quite well the exact (computed numerically) inversion of the relations (14) and (15). The worse error here is of about 3%, hence we conclude that our approach permits us to provide an accurate approximation of

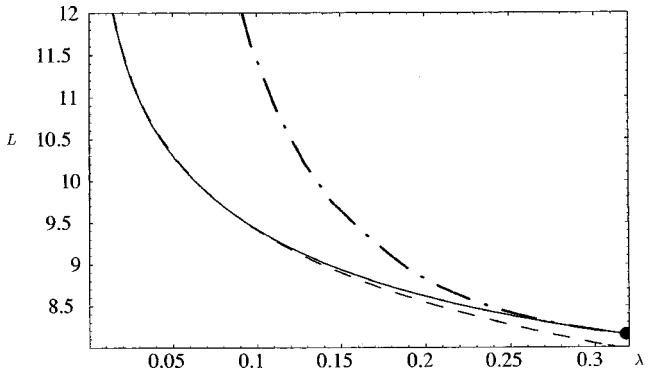

FIG. 5. Period L of the solution (13) vs λ. The solid line is the numerical evaluation of the period, and the dashed one corresponds to the approximation of large domain size $L^A(S,\lambda)$ [Eq. (18)]. The point-dashed line corresponds to the small domain approximation of the period $L_\varepsilon(S,\lambda)$ [Eq. (19)]. The full circle is the bifurcation point (λ_1^B, L_1^B).

the bifurcation branches for the Cahn-Hilliard equation for large domain and becomes quite good till the vicinity of the bifurcation point.

F. Small domain size

If we look at Fig. 3, we deduce that at $\lambda=\lambda_1^B$ the bubble solution emerges from the homogeneous one (u_b). When $\lambda<\lambda_1^B$, the spatial inhomogeneous solution is a perturbation of the homogeneous state. For this reason, for computing the solution near this point, we set the energy E of the mechanical system defined by the relation (9) to $E=V(u_b)+\epsilon$. By perturbation, one obtains the following roots of the polynomial $V(u)$:

$$u_1 = -u_b - \sqrt{2}\sqrt{1-u_b^2} + \eta_+\epsilon + o(\epsilon^{3/2}),$$

$$u_2 = u_b - \frac{1}{\sqrt{1-3u_b^2}}\sqrt{\epsilon} + \frac{u_b}{(1-3u_b^2)^2}\epsilon + o(\epsilon^{3/2}),$$

$$u_3 = u_b + \frac{1}{\sqrt{1-3u_b^2}}\sqrt{\epsilon} + \frac{u_b}{(1-3u_b^2)^2}\epsilon + o(\epsilon^{3/2}),$$

$$u_4 = -u_b + \sqrt{2}\sqrt{1-u_b^2} - \eta_-\epsilon + o(\epsilon^{3/2}),$$

where

$$\eta_\pm = (1+u_b^2 \mp 2u_b\sqrt{1-u_b^2})/[2\sqrt{2}(1-3u_b^2)^2\sqrt{1-u_b^2}].$$

Hence using the relations (14) and (15) we can determine the multibubble's period area near the bifurcation point

$$L_\epsilon(n) = \frac{n\pi}{\sqrt{1-3u_b^2}} + \frac{3n\pi(1+7u_b^2)}{8(1-3u_b^2)^{7/2}}\epsilon + o(\epsilon^{3/2}),$$

$$S_\epsilon(n) = \frac{2n\pi u_b}{\sqrt{1-3u_b^2}} - \frac{15n\pi u_b(1-u_b^2)}{4(1-3u_b^2)^{7/2}}\epsilon + o(\epsilon^{3/2}).$$

We are interested in the bifurcation lines for constant area S. We thus have $S_\epsilon(n)=L_n^B u_b^*(n)$. We then deduce that

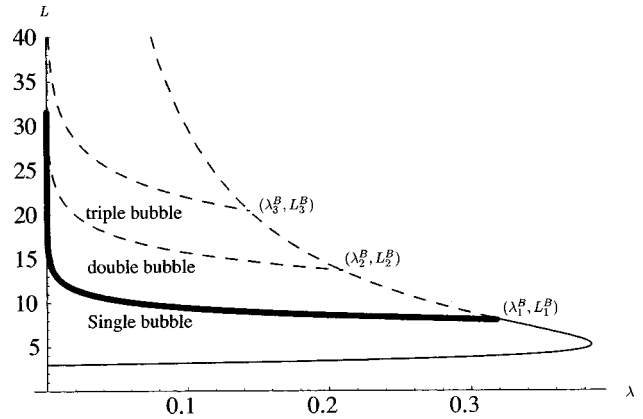

FIG. 6. Period L of the multibubble solution vs λ. The area value is $S=-3$. Periodic boundary conditions.

$$\epsilon = [u_b - u_b^*(n)]\frac{8[1-3u_b^{*2}(n)]^2}{15[u_b^{*2}(n)-1]},$$

$$S_\epsilon = \frac{2\pi u_b^*(n)}{\sqrt{1-3u_b^{*2}(n)}}.$$

We can now evaluate the approximation of the period of the solution:

$$L_\epsilon = L_n\left(1 + \frac{3(2n^2\pi^2 - S_\epsilon^2)L_n^2}{64n^4\pi^4}\epsilon + o(\epsilon^{3/2})\right). \qquad (19)$$

This result is compared with the numerical inversion of the relation (15) in Fig. 5, and the agreement is good in the vicinity of the bifurcation. From this relation we deduce that when $S_\epsilon^2<2\pi^2$, the slope of the bifurcation line (in the L-λ plane) is negative, and hence the bifurcation is supercritical. On the contrary, the bifurcation is subcritical, and bistability between a homogeneous state and a bubble solution is deduced.

In the case of bistability, according to the existence of a Lyapunov functional, a barrier separating two stable attractors is necessary. We relate this separatrix to an unstable manifold that permits the transition from homogeneous state to the bubble solution. Due to the intrinsic nature of the bifurcation, the spectrum of the linearized operator around the unstable solution must have just one positive eigenvalue, and its codimension-1 stable manifold acts as the potential barrier. The nucleation solution is therefore the unstable bubble that emerges from the subcritical bifurcation. For mathematical properties of the nucleation problem, see Refs. [34–36].

G. Unfolding the bifurcation, multibubble solution, and linear stability

In this section, we are interested in the scenario of bifurcation when the system size varies. As seen before, for each value of L_n, there is a bifurcation of the homogeneous state. From the bifurcation theory point of view, this means that there is appearance of a new branch of solutions as illustrated

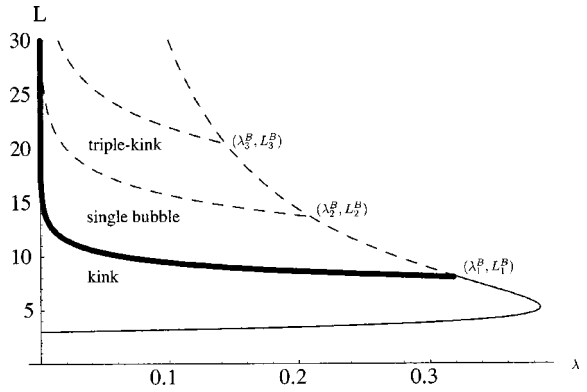

FIG. 7. Period L of the multibubbles solution vs λ. The area value is $S=-3$. Zero flux boundary condition.

in Fig. 6. In the previous section, we have related this new branch to a single bubble solution. Before the first bifurcation, u_b is stable, and if the bifurcation is supercritical, this means that in the new solution, the bubble is stable. In the other case, that is, for $S>\sqrt{2}\pi$, the bifurcation is subcritical, and the new solution is unstable.

Since at the nth bifurcation (11), the bifurcating u_b solution has $n-1$ strictly positive eigenvalues, the n-bubble solution is unstable. For a given area S, the n-bubble solution is composed of bubbles that have an area equal to $S_n=S/n$, and a period equal to $L_n^b=L/n$. Hence the stability is not affected far away from the bifurcation points, since there are no more possible bifurcations with other branches. This means that the unique stable spatial inhomogeneous solution with periodic boundary condition is the single bubble solution. The scenario of bifurcations is shown in Fig. 6

Now suppose that we set as an initial condition a perturbed bubble pair (symmetrical bubbles). Since the spectrum has one positive eigenvalue (if $S<\sqrt{8}\pi$), this means that the stable manifold of the solution is a separatrix in the functional space: two different behaviors are expected; this is clearly seen in the simulations and will be explained later in the context of bubble dynamics.

H. Scenario in the case of the Neumann boundary conditions

We have deduced the bifurcations scenario in the case of periodic boundary conditions. In the case of null flux boundary conditions, that is,

$$u_x = u_{xxx} = 0,$$

the kink solution is energetically favorable in comparison to the bubble solution, due to the energetic cost of interfacial tension. The bifurcations of the homogeneous state u_b observed in periodic geometry [Eq. (11)] are slightly changed, since the harmonic perturbations now take the form of $\cos[(n\pi/L)x]$. Hence the bifurcation points are

$$\begin{cases} L_n^B = \sqrt{3S^2 + n^2\pi^2}, \\ \lambda_n^B = -S\dfrac{2S^2 + n^2\pi^2}{(3S^2 + n^2\pi^2)^{3/2}}. \end{cases}$$

In Fig. 7 is represented the bifurcation diagram for this case, and we can then infer geometrically that the bubble solution is unstable, and has at least one strictly positive eigenvalue.

The bifurcation scenario and the counting of the solutions has been performed using quite different techniques in Ref. [39] and computed numerically in Ref. [45]. In the computation presented here, we managed to compute analytically the solutions and their bifurcation branches, up to an error which is exponentially small.

III. COARSENING DYNAMICS

The transient dynamics consisting in the formation of small domains that subsequently grow is denominated coarsening dynamics. In the last decades, extensive studies of the coarsening dynamics have been performed [32–35,42]. These approaches are based on an asymptotic reduction of the Cahn-Hilliard equation into a set of ODEs describing the evolutions of the positions of the kinks. We propose here an alternative way for deriving such ODEs. It is found that our reduced set of equations is different from the known ones [32–35], a fact that will be discussed at the end of this section. We first derive the set of ODEs for bubbles. Then we will study the special case of two interacting bubbles, and confront our prediction to the numerical results.

The query that we address now is how the system evolves to its global minimum. Previous to the global minimization of the free energy F, the system behaves minimizing locally the free energy in different regions of space yielding several bubbles. Hence we shall consider a gas of bubbles. The ith bubble is characterized by the position of its center x_i (the

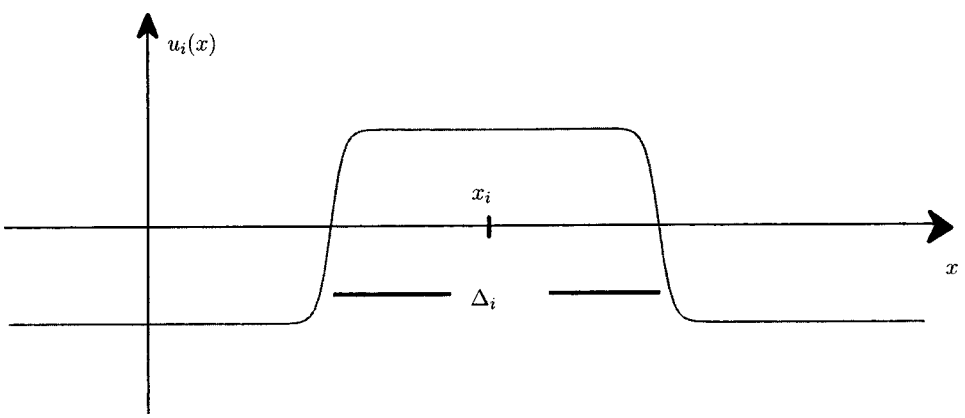

FIG. 8. Schematic representation of the bubble solution. x_i is the bubble center position and Δ_i is the width.

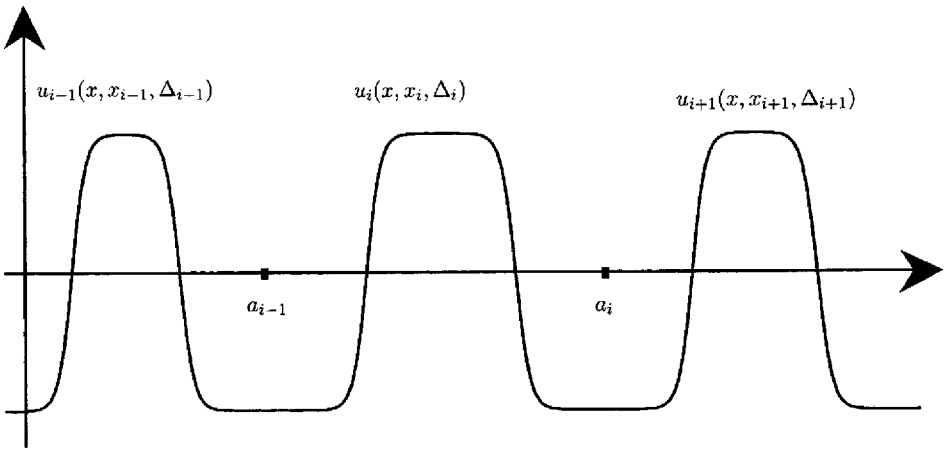

FIG. 9. Schematic representation of a diluted gas of bubbles. Each bubble is characterized by its position and its width. a_{i-1} represents an arbitrary intermediate fixed point between the $i-1$th and ith bubbles.

middle point between the two zeros of the bubble) and its width Δ_i (see Fig. 8).

Henceforth we consider a finite system size L larger than the bubble widths. In order to discern the different time scales involved in the system, we consider Eq. (7) in place of Eq. (8), where the bubble solutions have the following approximate form:

$$u_i(y) \approx -\sqrt{|\varepsilon|} + \sqrt{|\varepsilon|}\tanh\left[\sqrt{\frac{|\varepsilon|}{2}}\left(x - x_i + \frac{\Delta_i}{2}\right)\right] - \sqrt{|\varepsilon|}\tanh\left[\sqrt{\frac{|\varepsilon|}{2}}\left(x - x_i - \frac{\Delta_i}{2}\right)\right] + 4\sqrt{|\varepsilon|}e^{-\sqrt{2|\varepsilon|}\Delta} f(x), \tag{20}$$

where $f(x)$ is a bounded function that converges asymptotically to 1 when $x \to \pm\infty$, which has the form

$$f(x) = 1 - \frac{3}{2}\left\{\tanh\left[\sqrt{\frac{|\varepsilon|}{2}}\left(x - x_i + \frac{\Delta_i}{2}\right)\right] - \tanh\left[\sqrt{\frac{|\varepsilon|}{2}}\left(x - x_i - \frac{\Delta_i}{2}\right)\right]\right\} - \frac{3}{2}\sqrt{\frac{|\varepsilon|}{2}} \times \left\{\left(x - x_i + \frac{\Delta_i}{2}\right)\mathrm{sech}^2\left[\sqrt{\frac{|\varepsilon|}{2}}\left(x - x_i + \frac{\Delta_i}{2}\right)\right] - \left(x - x_i - \frac{\Delta_i}{2}\right)\mathrm{sech}^2\left[\sqrt{\frac{|\varepsilon|}{2}}\left(x - x_i - \frac{\Delta_i}{2}\right)\right]\right\}. \tag{21}$$

The parameter group $\{x_i, \Delta_i\}$ is determined by the initial conditions. The translation invariance and area conservation induce that the bubble solution has two Goldstone modes, that is, the spectrum of the linear operator (related to stability of the bubble solution) has two zero eigenvalues. The solutions of Eq. (7) are approximated as superposition of diluted bubbles (as is illustrated in Fig. 9): the separation between the bubbles is larger than their widths ($L \gg \Delta \gg 1/\sqrt{\varepsilon}$). Hence locally one has a bubble solution perturbed by the presence of the nearest ones, and the position of this bubble and its width are considered as variables. Since these variables have the slowest dynamical evolution, they lead to the asymptotic dynamics.

In order to find the evolution of these order parameters, we first integrate Eq. (7) from a_{i-1} to a_i and find

$$d_t \int_{a_{i-1}}^{a_i} u(x)dx = \partial_x \frac{\delta F}{\delta u}\bigg|_{a_{i-1}}^{a_i}, \tag{22}$$

where a_{i-1} is an intermediate arbitrary fixed point between the $i-1$th and ith bubbles (see Fig. 9) and $\partial_x(\delta F/\delta u)|_a^b \equiv \partial_x(\delta F/\delta u)|_b - \partial_x(\delta F/\delta u)|_a$. We associate the above integral with *the mass* of the ith bubble. In order to evaluate the left hand side of the above equation, we write

$$d_t \int_{a_{i-1}}^{a_i} u(x)dx = d_t \int_{a_{i-1}}^{a_i} \left[u(x) + \sqrt{|\varepsilon|}\,\right]dx.$$

Using the bubbles approximation (20), the dominant term of the integral takes the form

$$\int_{a_{i-1}}^{a_i} \left[u(x) + \sqrt{|\varepsilon|}\,\right]dx \approx 2\Delta_i\sqrt{|\varepsilon|},$$

then

$$d_t \int_{a_{i-1}}^{a_i} u(x)dx = 2\sqrt{|\varepsilon|}\partial_t\Delta_i$$

and Eq. (22), related to the bubble's width evolution, reads

$$2\sqrt{|\varepsilon|}\partial_t\Delta_i = \partial_x \frac{\delta F}{\delta u}\bigg|_{a_{i-1}}^{a_i}. \tag{23}$$

Similarly, we consider Eq. (7) multiplied by x and integrated in the same domain:

$$d_t \int_{a_{i-1}}^{a_i} xu(x)dx = x\partial_x \frac{\delta F}{\delta u}\bigg|_{a_{i-1}}^{a_i} - \frac{\delta F}{\delta u}\bigg|_{a_{i-1}}^{a_i}.$$

This integral is related to the motion of the center of the mass of the ith bubble. Evaluating the integral in the left hand side of the above equation we obtain at dominant order

$$\int_{a_{i-1}}^{a_i} x[u(x) + \sqrt{|\varepsilon|}]dx \approx 2\sqrt{|\varepsilon|}x_i\Delta_i.$$

Hence

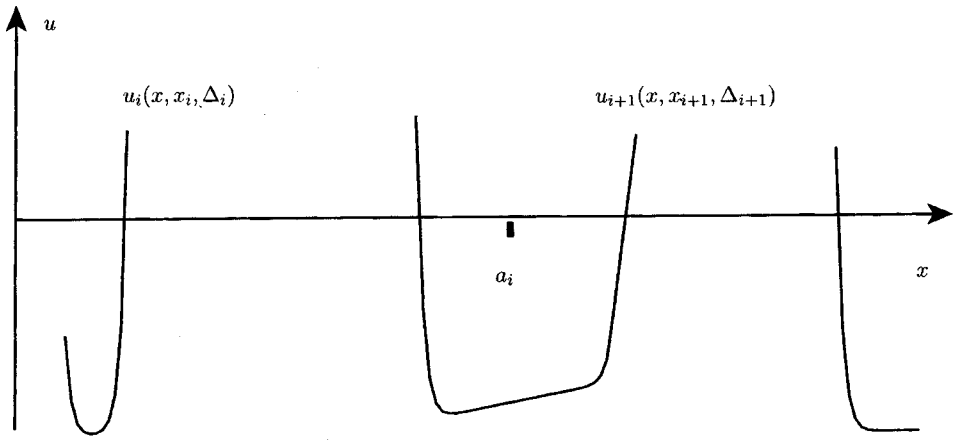

FIG. 10. Schematic representation of the enlarged interbubble region.

$$\frac{d}{dt}\int_{a_{i-1}}^{a_i} xu(x)dx = 2\sqrt{|\varepsilon|}\frac{d(x_i\Delta_i)}{dt} = x\partial_x\frac{\delta F}{\delta u}\bigg|_{a_{i-1}}^{a_i} - \frac{\delta F}{\delta u}\bigg|_{a_{i-1}}^{a_i}. \tag{24}$$

Using the identity

$$\begin{aligned} x\partial_x\frac{\delta F}{\delta u} - \frac{\delta F}{\delta u}\bigg|_{a_{i-1}}^{a_i} &= \left[\frac{\delta F}{\delta u}\bigg|_{a_{i-1}} + \partial_x\frac{\delta F}{\delta u}\bigg|_{a_{i-1}}\left(x_i - \frac{\Delta_i}{2} - a_{i-1}\right)\right] \\ &\quad - \left[\frac{\delta F}{\delta u}\bigg|_{a_i} + \partial_x\frac{\delta F}{\delta u}\bigg|_{a_i}\left(x_i + \frac{\Delta_i}{2} - a_i\right)\right] \\ &\quad - \left(x_i - \frac{\Delta_i}{2}\right)\partial_x\frac{\delta F}{\delta u}\bigg|_{a_{i-1}} \\ &\quad + \left(x_i + \frac{\Delta_i}{2}\right)\partial_x\frac{\delta F}{\delta u}\bigg|_{a_i}, \end{aligned} \tag{25}$$

and the fact that the intermediate region, between the bubbles, is a straight line (as illustrated in Fig. 10) we can approximate

$$\begin{aligned} \frac{\delta F}{\delta u}\bigg|_{x_i-\Delta_i/2} &\approx \left[\frac{\delta F}{\delta u}\bigg|_{a_{i-1}} + \partial_x\frac{\delta F}{\delta u}\bigg|_{a_{i-1}}\left(x_i - \frac{\Delta_i}{2} - a_{i-1}\right)\right], \\ \frac{\delta F}{\delta u}\bigg|_{x_i+\Delta_i/2} &\approx \left[\frac{\delta F}{\delta u}\bigg|_{a_i} + \partial_x\frac{\delta F}{\delta u}\bigg|_{a_i}\left(x_i + \frac{\Delta_i}{2} - a_i\right)\right]. \end{aligned} \tag{26}$$

In the above expressions, we have neglected the exponential corrections and obtain

$$\begin{aligned} x\partial_x\frac{\delta F}{\delta u} - \frac{\delta F}{\delta u}\bigg|_{a_{i-1}}^{a_i} &\approx \frac{\delta F}{\delta u}\bigg|_{x_i-\Delta_i/2} - \frac{\delta F}{\delta u}\bigg|_{x_i+\Delta_i/2} \\ &\quad - x_i\left(\partial_x\frac{\delta F}{\delta u}\bigg|_{a_i-1} - \partial_x\frac{\delta F}{\delta u}\bigg|_{a_i}\right) \\ &\quad + \frac{\Delta_i}{2}\left(\partial_x\frac{\delta F}{\delta u}\bigg|_{a_i-1} + \partial_x\frac{\delta F}{\delta u}\bigg|_{a_i}\right). \end{aligned}$$

The positions $x_i \pm \Delta_i/2$ are the roots of the bubble solution, that is, $u_i(x_i \pm \Delta_i/2) = 0$. The variation of the free energy $(\delta F/\delta u)$ at these points are the same, then

$$\begin{aligned} 2\sqrt{|\varepsilon|}\frac{d(x_i\Delta_i)}{dt} &= -x_i\left(\partial_x\frac{\delta F}{\delta u}\bigg|_{a_{i-1}} - \partial_x\frac{\delta F}{\delta u}\bigg|_{a_i}\right) \\ &\quad + \frac{\Delta_i}{2}\left(\partial_x\frac{\delta F}{\delta u}\bigg|_{a_{i-1}} + \partial_x\frac{\delta F}{\delta u}\bigg|_{a_i}\right). \end{aligned}$$

Using Eq. (23) we find

$$\partial_t x_i = \frac{1}{4\sqrt{|\varepsilon|}}\left(\partial_x\frac{\delta F}{\delta u}\bigg|_{a_{i-1}} + \partial_x\frac{\delta F}{\delta u}\bigg|_{a_i}\right).$$

At dominant order the equations for the bubble's position and the bubble's width are functions of $\partial_x(\delta F/\delta u)$, which has the form

$$\partial_x\frac{\delta F}{\delta u} = \varepsilon u_x + 3u^2u_x - u_{xxx}.$$

The bubble solution at a_i and a_{i-1} has the form $u \approx -\sqrt{|\varepsilon|} + O(|\varepsilon|^{1/2}e^{-\sqrt{2|\varepsilon|}\Delta_i})$, thus we can approach

$$\partial_x\frac{\delta F}{\delta u}\bigg|_{a_i} \approx 2|\varepsilon|u_x(a_i),$$

therefore the dynamics of bubble's position and bubble's width are

$$\begin{aligned} \partial_t\Delta_i &= \sqrt{|\varepsilon|}[u_x(a_i) - u_x(a_{i-1})], \\ \partial_t x_i &= \frac{\sqrt{|\varepsilon|}}{2}[u_x(a_i) + u_x(a_{i-1})]. \end{aligned} \tag{27}$$

Since each bubble's tail converges asymptotically to $-\sqrt{|\varepsilon|}$ as a function of its width, a well defined tilt between the bubbles is established, as illustrated in Fig. 10. Hence if the ith bubble is surrounded by two bubbles with smaller widths, then $u_x(a_i)$ is positive and $u_x(a_{i-1})$ is negative, then the ith bubble width grows in time $(\partial_t\Delta_i > 0)$.

A simple approximation of the tilt is

$$\partial_x u(a_{i-1}) \approx \frac{u_i\left(x_i - \frac{\Delta_i}{2}\right) - u_{i-1}\left(x_{i-1} + \frac{\Delta_{i-1}}{2}\right)}{\left(x_i - \frac{\Delta_i}{2}\right) - \left(x_{i-1} + \frac{\Delta_{i-1}}{2}\right)}.$$

Using expression (20) one reads

$$\partial_x u(a_{i-1}) \approx \frac{4\sqrt{|\varepsilon|}(e^{-\sqrt{2|\varepsilon|}\Delta_i} - e^{-\sqrt{2|\varepsilon|}\Delta_{i-1}})}{x_i - x_{i-1} - \frac{\Delta_i + \Delta_{i-1}}{2}}$$

$$= \frac{8\sqrt{|\varepsilon|}e^{-\sqrt{|\varepsilon|/2}(\Delta_{i-1}+\Delta_i)}}{x_i - x_{i-1} - \frac{\Delta_i + \Delta_{i-1}}{2}} \sinh\left[\sqrt{\frac{|\varepsilon|}{2}}(\Delta_{i-1} - \Delta_i)\right].$$

Introducing the function

$$I_{i,i-1}(\varepsilon, \Delta_{i-1}, \Delta_i) = \frac{8\sqrt{|\varepsilon|}e^{-\sqrt{|\varepsilon|/2}(\Delta_{i-1}+\Delta_i)}}{x_i - x_{i-1} - \frac{\Delta_i + \Delta_{i-1}}{2}} \times \sinh\left[\sqrt{\frac{|\varepsilon|}{2}}(\Delta_{i-1} - \Delta_i)\right],$$

the width and position equations take the form [47]

$$d_t \Delta_i = I_{i+1,i} - I_{i,i-1},$$

$$d_t x_i = \frac{I_{i+1,i} + I_{i,i-1}}{2}. \tag{28}$$

We remark that these equations are invariant by the transformations

$$\Delta_i \to \Delta_i + \alpha,$$

$$x_i - x_{i-1} \to x_i - x_{i-1} + \alpha,$$

$$t \to t \exp(\sqrt{2|\varepsilon|}\alpha),$$

where α is an arbitrary constant. Due to this invariance the average $\langle \Delta(t) \rangle = (1/n)\Sigma\Delta_i$, which is a function of time, satisfies the similarity relation $\Delta(t) + \alpha = \Delta(t \exp(\sqrt{2|\varepsilon|}\alpha))$. From this relation we conclude that

$$\Delta(t) = \frac{1}{\sqrt{2|\varepsilon|}} \ln t,$$

i.e., we recuperate in a very simple way the logarithmic increase with time of the average separation of the bubbles [32,42], which has recently been observed experimentally [13]. It is remarkable that to obtain this behavior one does not need to have an explicit solution since in our approach it is an exact consequence of a symmetry of our reduced equations of motion. Note that the dynamics of the bubble's position and bubble's width is independent of the arbitrary intermediate fixed points a_i. If we consider a system of size L with periodic boundary conditions and n bubbles, the above equations describe the dynamics of bubbles' widths and bubble's positions with the conditions

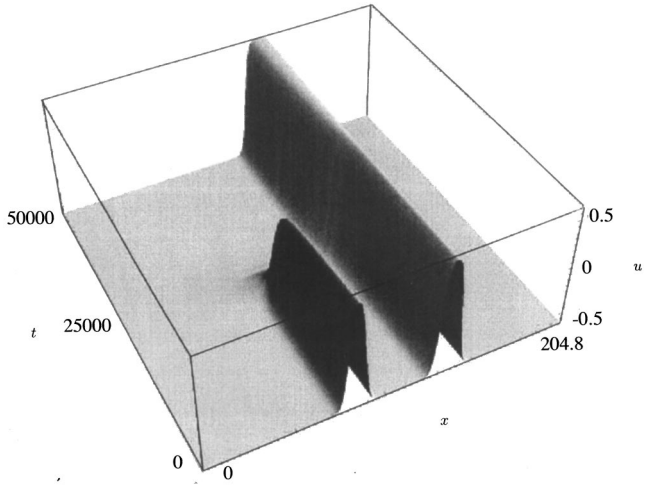

FIG. 11. Spatiotemporal evolution of two bubbles with different size. Numerical simulation of the Cahn-Hilliard equation with $\epsilon = -0.25$, initial total area $S = -81.50$, $\Delta_1 = 9.16$, and $\Delta_2 = 14.46$.

$$\Delta_{n+1} = \Delta_1, \quad \Delta_o = \Delta_n,$$

$$x_{n+1} = x_1 + L, \quad x_o = x_n - L,$$

and

$$I_{n+1,n} = I_{1,0} = \frac{8\sqrt{|\varepsilon|}e^{-\sqrt{2|\varepsilon|}(\Delta_n+\Delta_1)}}{x_i - x_{i-1} - \frac{\Delta_i + \Delta_{i-1}}{2}} \sinh\left[\sqrt{\frac{|\varepsilon|}{2}}(\Delta_n - \Delta_1)\right].$$

If the lateral bubbles are thinner (respectively wider) than the central one, the latter width increases (respectively decreases), as shown in Fig. 11. Therefore the larger bubbles increase as a consequence of the disappearance of their thinner neighbors, and in such a way that the global area is conserved for periodic boundary conditions ($d_t \Sigma \Delta_i = 0$). The bubbles' interaction depends on the inverse of the distance between them and exponentially with their widths. When the bubbles are close enough, our description loses its validity. In this circumstance, the dynamics of the system is given by Eqs. (28) by means of *complementary bubbles* as we shall see later.

A. Two bubbles

To illustrate the dynamics given by Eq. (23), we consider the case of two bubbles with periodic boundary conditions. Prior to the establishment of the stationary state, which corresponds to the global minimum of the free energy, the dynamics is led by the two bubbles interaction

$$-d_t \Delta_2 = d_t \Delta_1 = I_{2,1} - I_{1,2},$$

$$d_t(x_1 \Delta_1 + x_2 \Delta_2) = L I_{1,2},$$

$$d_t x_2 = d_t x_1 = \frac{I_{2,1} + I_{1,2}}{2}, \tag{29}$$

where L is the system size. The first equations express the conservation of the area at dominant order. The second equa-

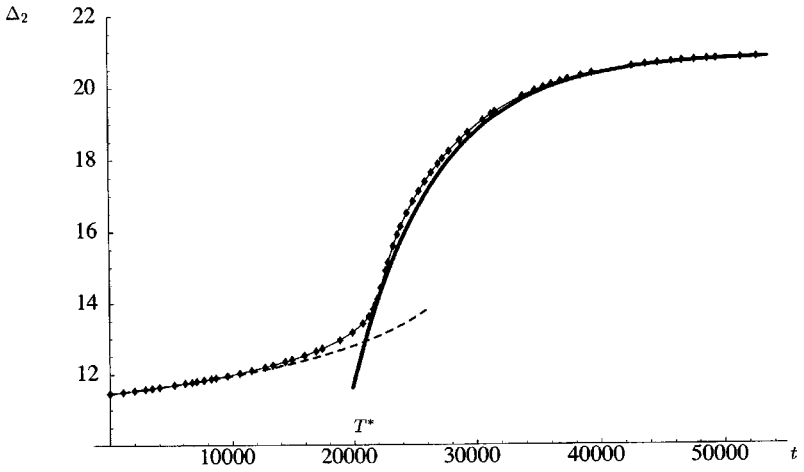

FIG. 12. Temporal evolution of the bubble's width obtained from the simulation and from the analytical approximations. The symbol line is obtained from numerical simulation of the Cahn-Hilliard model with $\epsilon=0.25$, the dashed line is obtained from the expression (32), and solid thick line is obtained using the analytical expression of the relaxation dynamics (31).

tion tells us that the global *center of mass* moves in the direction of the largest bubble. We note that the case of identical bubbles is an unstable stationary state ($\Delta_1=\Delta_2$) whose stable manifold is a separatrix in the functional phase space, as we have shown in Sec. II G. Due to the translation invariance of the system, the more appropriate order parameter that describes the interaction is the distance between the bubbles. Using the previous equations we obtain

$$d_t(x_2 - x_1) = 0.$$

So, at dominant order the distance between the bubbles is constant. Numerically, we observe that bubbles move slowly. In order to find this dynamic, one can take into account the solvability condition of the two bubbles solution [32–35] and use the dynamics of the bubble's width (29). The first correction of the previous equations takes the form

$$d_t(x_2 - x_1) = -|\varepsilon|^{1/2}(I_{2,1} + I_{1,2})\frac{(\Delta_1 - \Delta_2)}{\Delta_1\Delta_2}. \qquad (30)$$

This equation indicates to us that the bubbles always attract themselves, i.e., the distance (the smallest one) between them always decreases and the interaction law depends on the inverse of the distance (see the definition of $I_{1,2}$), but the intensity of this effect is $|\varepsilon|$ smaller than the evolution of the other quantities ($\Delta \sim 1/|\varepsilon|^{-1/2}$). Therefore the bubbles interact mainly through their widths (see Fig. 11) and the widest bubble increases its width and moves slightly towards the thinnest one. Numerical simulations confirm this description as shown in Fig. 11. In Fig. 12, we compare the evolution of $\Delta_2(t)$ obtained through numerical integration of the Cahn-Hilliard equation with the analytical one [Eq. (29)], and we find good agreement.

Despite the fact that we have done many approximations, a good agreement is found with the simulations. We compare numerically and analytically the spatial derivative of the field $u(x,t)$ at intermediate points between the bubbles and find

$$\partial_x u(a)_{\text{numeric}} = -2.69 \times 10^{-8},$$

$$\partial_x u(a) = I_{i+1,i} = -2.60 \times 10^{-8},$$

i.e., an error of 3.5%. The error in the width and the position dynamics [Eq. (29)] is 4.2 and 17.3%, respectively. This emphasizes that Eqs. (29) and (30) give qualitatively and quantitatively the evolution of the ulterior dynamics.

The previous description seems to be valid when the bubbles are sufficiently separated ($x_1 - x_2 > \Delta_1, \Delta_2$ and $\Delta_{1,2} \gg \sqrt{|\varepsilon|}$). If the bubbles are close enough, as illustrated in Fig. 13, one can also use the preceding description but using now the complementary bubbles which are related to the original bubbles obtained through the transformation $u(x,t) \rightarrow -u(x,t)$ (cf. Fig. 13).

Using Eqs. (29) and (30) for the complementary bubbles we find that in the original field $[u(x,t)]$, the closest bubbles get near and finally merge. These two qualitatively different dynamics result from the existence of a separatrix in the functional space as shown in Sec. II G. Therefore the interaction laws (29) and (30) allow us to describe the evolution of diluted bubbles or nearest ones by consideration of the appropriate bubbles, i.e., the complementary or the original ones.

As we have seen in Sec. II H the bubble solution with null flux boundary conditions is unstable. It moves toward the nearest border and finally disappears giving rise to a kink solution [43]. In the case for which the bubble is exactly in the center of the system, a very small perturbation may *push* the bubble in one direction or the other: this reflects the existence of the stable manifold of codimension 1 predicted in Sec. II H. In order to calculate the bubble velocity we use the image method doubling the size of the system. The original bubble gives rise to two bubbles by reflection in the midpoint and we finally have a system of double length with two bubbles and periodic boundary conditions. Since the bubbles are equal, Eqs. (29) do not give directly the dynamics and it is necessary to use the complementary bubbles for which Eqs. (29) are not trivial. One obtains that the bubble width dynamics is double the pursuit velocity and then

$$\partial_t x = \frac{8|\varepsilon|e^{-\sqrt{2|\varepsilon|}(L-\Delta)}}{\Delta}\sinh\left[\sqrt{2|\varepsilon|}\left(x - \frac{L}{2}\right)\right],$$

where (Δ, x) are the bubble width and position, respectively. If the bubble width is of order $|\varepsilon|^{1/2}$, our description loses its validity.

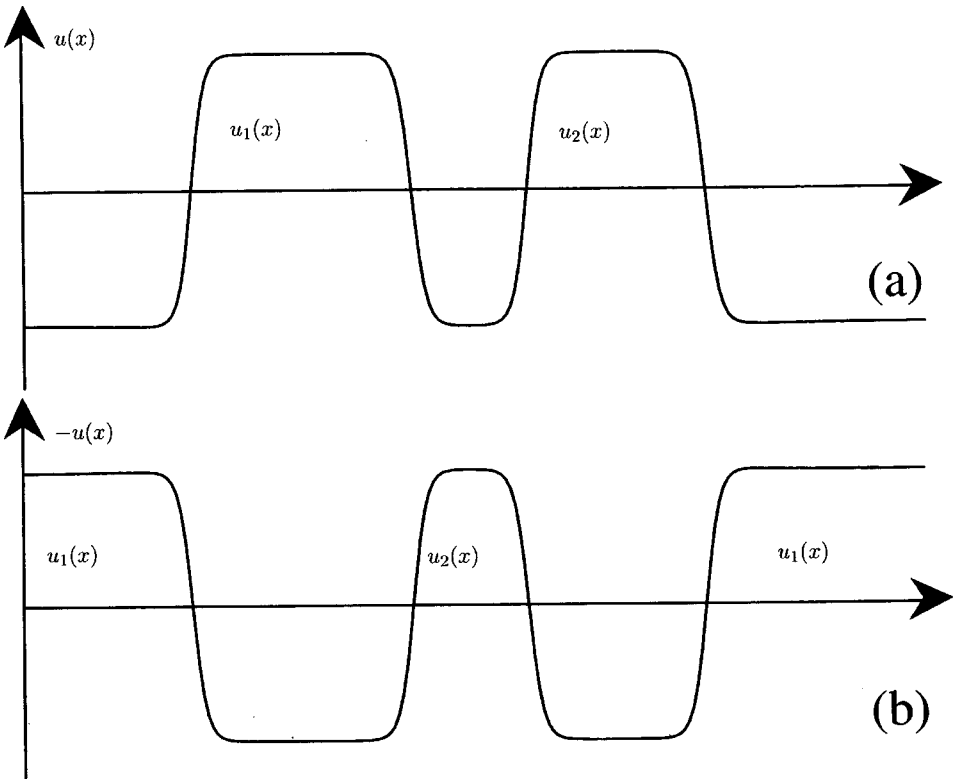

FIG. 13. Schematic representation of (a) the bubble solutions and (b) the complementary ones.

B. Relaxation dynamics

For time less than T^* (see Fig. 12) the dynamics is led by the interaction laws (29) and (30). For times larger than T^*, the system relaxes to the global minimum. Once the smallest bubble disappears, the system is described by one perturbed bubble. Thus the dynamics is characterized by exponential relaxation to the bubble solution (20). One can determine this characteristic time by means of a simple linear analysis of the bubble solution. The perturbation of one bubble solution u_o with width Δ in a system of size L is described by

$$\sigma v = \partial_{yy}[-\epsilon + 3u_0(x)^2 - \partial_{xx}]v,$$

where $u(x,t)=u_o(x)+v(x)e^{\sigma t}$ and $|v| \ll |u_o|$. Another way to study the stability of the (multi)bubble consists of computing the second variation of the free energy; this has the advantage of allowing a complete analysis [48]. It is possible to compute approximately the continuous part of the spectrum, which contains the eigenvalues whose eigenvectors do not converge to zero at infinity. Far away from the bubble's position, the field u_0 asymptotically converges to u_1 at $\pm\infty$. Then the spectrum must also obey

$$\sigma v = \partial_{yy}(-\epsilon + 3u_1^2 - \partial_{xx})v.$$

Making Fourier expansion with spatial frequency p, the eigenvalues satisfy

$$\sigma v = -p^2(-\epsilon + 3u_1^2 + p^2)v.$$

When the bubble's width is large enough, $u_1 \approx -\sqrt{\epsilon}$ and the eigenvalues are $\sigma=-p^2(2\epsilon+p^2)$, the spatial frequencies p is approximated by

$$p \approx \frac{n\pi}{L-\Delta},$$

since the bubble's width Δ imposes an effective periodic domain of size $(L-\Delta)$. The eigenvalues are approximated by

$$\sigma \simeq -\frac{n^2\pi^2}{(L-\Delta)^2}\left(2\epsilon + \frac{n^2\pi^2}{(L-\Delta)^2}\right), \tag{31}$$

with nonlocalized eigenvector. This rough approximation permits us to compute the eigenvalues with a quite reasonable agreement with the numerical simulations, as depicted in Fig. 14. We emphasize that this derivation is an analog of the WKB method. Moreover, numerical computations show that the tails of these eigenvectors are similar to the harmonics one derived above (cf. Fig. 14).

This continuous spectrum plays a fundamental role in the bubble dynamics, because the bubble disappearance creates a large perturbation far away from its position and excites these modes.

C. Analytical solution of two bubbles' interaction

When one considers the dynamics of the bubble's width and the bubble's position (29), it is found that $\Delta_1+\Delta_2=\Delta$ and $x_2-x_1=R$ are constants. We introduce the auxiliary variable $\delta \equiv \Delta_1-\Delta_2$ which satisfies

$$d_t\delta = 2(I_{2,1} - I_{1,2})$$

or equivalently

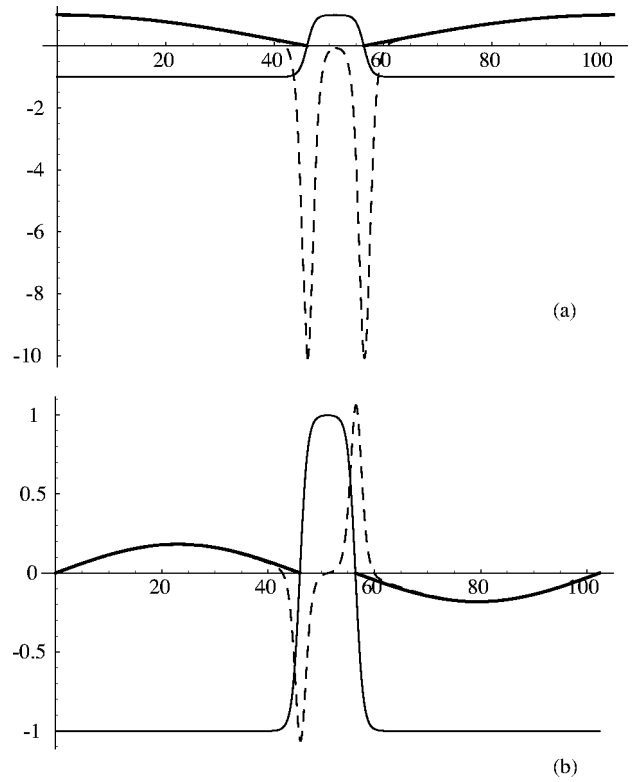

FIG. 14. Comparison of numerical eigenvector and the approximated ones. The dashed line is the numerical eigenvector, the thick line is the approximated one, and the solid line is the bubble solution with $\lambda=3.062\times10^{-6}$, $\epsilon=-1$, and system size $L=102.4$. (a) First eigenvector with numerical eigenvalue -0.0023 and approximated to -0.0024 using expression (31). (b) Second eigenvector numerical eigenvalue -0.0093 and approximated to -0.0097 using expression (31).

$$d_t\delta = 2C\sinh\left[\sqrt{\frac{|\varepsilon|}{2}}\delta\right],$$

where C is a constant defined

$$C = \frac{8|\varepsilon|(L-\Delta)e^{-\sqrt{|\varepsilon|/2}\Delta}}{\left(R-\frac{\Delta}{2}\right)\left(L-R-\frac{\Delta}{2}\right)}.$$

The solution of the above equation is

$$\delta(t) = 2\sqrt{\frac{2}{|\varepsilon|}}\,\mathrm{arctanh}\left(\tanh\left[\frac{1}{2}\sqrt{\frac{|\varepsilon|}{2}}\delta_o\right]e^{\sqrt{2|\varepsilon|}C(t-t_o)}\right)$$

with $\delta(t_o)=\delta_o$. Then the widths take the form

$$\Delta_1 = \frac{\Delta+\delta(t)}{2},$$

$$\Delta_2 = \frac{\Delta-\delta(t)}{2}. \tag{32}$$

In Fig. 12, numerical simulations are compared with the previous solutions. The time when one bubble disappears (T^*) can be determined from the above expressions. For the sake of simplicity, we consider the case $\Delta_1<\Delta_2$, then

$$T^* = t_o + \frac{1}{C\sqrt{2|\varepsilon|}}\ln\left|\frac{\tanh\left[\frac{1}{2}\sqrt{\frac{|\varepsilon|}{2}}\Delta\right]}{\tanh\left[\frac{1}{2}\sqrt{\frac{|\varepsilon|}{2}}\delta\right]}\right|,$$

where $\Delta_2(T^*)=\Delta$ or $\Delta_1(T^*)=0$. We note that this time decreases when the bubbles are more dissimilar, whereas it becomes infinite when the widths are the same, since it is a stationary unstable state. Besides, this time increases with the total width Δ.

The evolution of the bubble's positions are given by

$$d_t x_1 = d_t x_2 = \frac{I_{2,1}+I_{1,2}}{2} = \frac{L-2R}{2(L-\Delta)}d_t\Delta_1$$

and using the expression of $\Delta_1(t)$ we obtain

$$x_1(t) = x_1(t_o) - \frac{L-2R}{2(L-\Delta)}\left[\frac{\delta_o-\delta(t)}{2}\right],$$

$$x_2(t) = x_2(t_o) - \frac{L-2R}{2(L-\Delta)}\left[\frac{\delta_o-\delta(t)}{2}\right].$$

The distance between the bubbles is constant, however, the position of the greatest bubble moves to the smallest one and the smallest moves away from the greatest one. For small time $[\sqrt{2|\varepsilon|}C(t-t_o)\ll1]$ the width changes proportionally to the time, i.e., $\Delta_{1,2}\sim t$ as shown in Fig. 11.

D. Comparison of our model with the Kawasaki-type equations

As argued in the beginning of the section, extensive studies have been devoted to derive a set of ODEs predicting the dynamics of the bubbles [32–35]. These calculations are based on the assumption that the kink-antikink pairs are sufficiently diluted, a hypothesis we also use. The technique for the reduction to an ODE is a Fredholm alternative. Two approaches have been used. In the first case [32,33], the compatibility condition is applied over an autoadjoint operator (obtained by inversion of the Laplacian operator), and in the second case, over a nonautoadjoint operator [34,35]. Both computations give rise to the same set of ODEs. In our case, the reduction is done by a study of the dynamics of the mass and the position of the bubbles, and no Fredholm alternative is used. Here we take into account the fact that in between the kinks the field is slightly tilted (see Fig. 10), whereas in the former works, the field is seen as constant. This tilt is explained as the following: the kink solution asymptotically converges at $\pm\infty$ to $-\sqrt{|\varepsilon|}$, but the bubble solution converges to a value that depends on its width $[-\sqrt{|\varepsilon|}+o(\sqrt{|\varepsilon|})\exp-(\sqrt{2|\varepsilon|}\Delta)]$ as seen in Eq. (17). This small difference leads to the dynamics. In particular for the two bubble coarsening, following the former works [32–35], one can deduce that the evolution of the distance $d=x_2-x_1-\frac{1}{2}(\Delta_2+\Delta_1)$ between the interacting bubbles is of the same order as the evolution of the widths, whereas we claim that it is a second-order effect

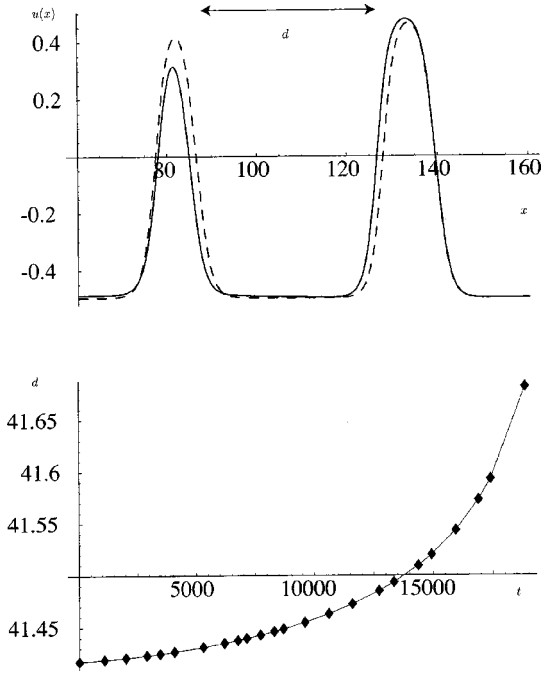

FIG. 15. Distance separating two bubbles. (a) Two snapshots of the field u taken at time $t=0$ for the solid line and $t=18\,876$ for the dashed one. In (b) we plot the distance between the zeros of the field u defined with $d=x_2-x_1-\frac{1}{2}(\Delta_2+\Delta_1)$

(order $|\varepsilon|$) as stated in Eq. (30). Numerical calculations support our prediction. In Fig. 15, it is seen that the variation of d is of order 0.7%, whereas the change in area of the biggest bubble (seen in Fig. 12) is of order 8%. We have taken the correction (30) for d, and integrated it. The relative error with the direct simulation becomes less than 1%.

The dynamics of the bubble widths obtained in Refs. [32–35] are qualitatively the same as ours. And it is from their equations that is deduced the logarithmic behavior in time of the characteristic length scale. This law has been deduced theoretically in Ref. [42] from the Cahn-Hilliard equation and recently verified experimentally [13]

IV. CONCLUSION

A traditional model used in the description of conservative phase separation is the Cahn-Hilliard system. In the frame of interface instability for two-dimensional extended systems, one can find that the dynamics of an interface which connects two symmetrical domains is described by the one-dimensional Cahn-Hilliard model, where the conservative order parameter is the spatial variation of interface's position, and the conservative quantity is the interface's area with respect to the initial flat interface.

We have studied the dynamics of the one-dimensional Cahn-Hilliard model, which is characterized by relaxation dynamics described by a free energy (Lyapunov potential). We have persued the stationary solutions of this model and established the local and global minima. The bifurcation scenarios of these stationary solutions as functions of the initial area and system size have been studied. These bubbles are characterized by the parameter group position and width. In order to describe the ulterior dynamics of one-dimensional Cahn-Hilliard model, we have considered a gas of diluted bubbles and found a set of ordinary differential equations, which describes the interactions between them. These equations allowed us to give a simple description of the coarsening dynamics observed in the system, in terms of the bubble's position and bubble's width. In order to illustrate the asymptotic dynamics, we have considered the case of two bubbles with periodic boundary conditions. We have deduced explicitly the behavior of the position and the width of the bubbles. We confronted our prediction with those obtained in Refs. [32–35] and conclude that different dynamics are predicted. For example, for the interaction of two bubbles, our conclusions are validated by numerical simulations. After the interaction, we show that the relaxation dynamics leads the system.

ACKNOWLEDGMENTS

The simulation software developed at the laboratory INLN in France has been used for all the numerical simulations presented in this paper. The authors thank the support of FONDAP (Grant No. 11980002), ECOS, and the CNRS-CONICYT cooperation program. M.G.C. thanks the support of Programa de inserción de científicos Chilenos of Fundación Andes, FONDECYT (Project No. 1020782), and Ayuda a la investigación of University of Los Andes ICIV-001-02. M.A. and E.T. acknowledge support of FONDECYT (Project Nos. 3000017 and 1020374, respectively).

[1] M. Cross and P. Hohenberg, Rev. Mod. Phys. **65**, 851 (1993).
[2] J. S. Langer, Rev. Mod. Phys. **52**, 1 (1980), and all references therein.
[3] *Growth and Form—Non Linear Aspects*, edited by M. Ben Amar *et al.* (Plenum Press, New York, 1991).
[4] J. A. Sethian, *Level Set Methods and Fast Marching Methods: Evolving Interfaces in Computational Geometry, Fluid Mechanics, Computer Vision, and Materials Science* (Cambridge University Press, New York, 1999).
[5] D. M. Petrich and R. E. Goldstein, Phys. Rev. Lett. **72**, 1120 (1994); R. E. Goldstein, D. J. Muraki, and D. M. Petrich, Phys. Rev. E **53**, 3933 (1996).
[6] R. C. Brower, D. A. Kessler, J. Koplik, and H. Levine, Phys. Rev. Lett. **51**, 1111 (1983).
[7] J. Burgers, Adv. Appl. Mech. **1**, 171 (1948).
[8] Y. Kuramoto and T. Tsuzuki, Prog. Theor. Phys. **55**, 356 (1976).
[9] G. I. Sivashinsky, Acta Astronaut. **4**, 1177 (1977).
[10] P. Clavin, Prog. Energy Combust. Sci. **11**, 1 (1985); P. Pelcé and P. Clavin, J. Fluid Mech. **124**, 219 (1982); F. Sabathier, L.

Boyer, and P. Clavin, Prog. Astronaut. Aeronaut. **76**, 246 (1981); G. I. Sivashinsky, Annu. Rev. Fluid Mech. **15**, 179 (1983).
[11] A. Hubert and R. Schafer, *Magnetic Domains* (Springer-Verlag, Berlin, Heidelberg, 1998).
[12] L. N. Bulaevskii and V. L. Ginzburg, Zh. Eksp. Teor. Fiz. **45**, 772 (1963) [Sov. Phys. JETP **18**, 530 (1964)]; P. Coullet, J. Lega, B. Houchmanzadeh, and J. Lajzerowicz, Phys. Rev. Lett. **65**, 1352 (1990).
[13] T. Nagaya and J. M. Gilli, Phys. Rev. E **65**, 051708 (2002).
[14] J. W. Cahn and J. E. Hilliard, J. Chem. Phys. **28**, 258 (1958).
[15] J. S. Langer, Ann. Phys. (N.Y.) **65**, 53 (1971).
[16] S. de Fontaine, *Ultrafine-Grain Metals* (Syracuse University Press, New York, 1971).
[17] A. J. Schwartz, J. S. Huang, and W. I. Goldberg, Chem. Phys. **62**, 1847 (1975).
[18] L. Granasy, T. Pusztai, and P. F. James, J. Chem. Phys. **117**, 6157 (2002).
[19] C. A. Smolders, J. J. van Aartsen, and A. Steenbergen, Kolloid Z. Z. Polym. **242**, 14 (1971).
[20] P. Manneville and J.-M. Piquemal, Phys. Rev. A **28**, 1774 (1983).
[21] R. Ribotta, A. Joets, and Lin Lei, Phys. Rev. Lett. **56**, 1595 (1986); E. Bodenschatz, M. Kaiser, L. Kramer, W. Pesch, A. Weber, and W. Zimmermann, *New Trends in Nonlinear Dynamics and Pattern-Forming Phenomena*, edited by P. Coullet and P. Huerre (Plenum Press, New York, 1990).
[22] C. Chevallard, M. Clerc, P. Coullet, and G. J. Gilli, Eur. Phys. J. E **1**, 179 (2000).
[23] C. Chevallard, M. Clerc, P. Coullet, and G. J. Gilli, Europhys. Lett. **58**, 686 (2002).
[24] Yu. A. Astrov, E. Ammelt, and H. G. Purwins, Phys. Rev. Lett. **78**, 3129 (1997).
[25] R. Ragnarsson, J. L. Ford, C. D. Santangelo, and E. Bodenschatz, Phys. Rev. Lett. **76**, 3456 (1996).
[26] L. Limat, Europhys. Lett. **44**, 205 (1998).
[27] C. Elphick, G. R. Ierley, O. Regev, and E. A. Spiegel, Phys. Rev. A **44**, 1110 (1991).
[28] D. K. Campbell, A. C. Newell, R. J. Schreiffer, and H. Segur, Physica D **18**, 1 (1986).
[29] B. A. Malomed and A. A. Nepomnyashchy, Phys. Rev. A **42**, 6009 (1990).
[30] D. Mermin, Rev. Mod. Phys. **51**, 591 (1979).
[31] K. Kawasaki, Prog. Theor. Phys. **79**, 161 (1984); **80**, 123 (1984).
[32] T. Kawakatsu and T. Munakata, Prog. Theor. Phys. **64**, 11, 1985.
[33] K. Kawasaki and T. Otha, Physica A **116**, 573 (1982); T. Nagi and K. Kawasaki, *ibid.* **139**, 438 (1986).
[34] P. W. Bates and J. Xun, J. Diff. Eqns. **111**, 421 (1994).
[35] P. W. Bates and J. Xun, J. Diff. Eqns. **117**, 165 (1995).
[36] A. Novick-Cohen and L. A Segel, Physica D **10**, 277 (1984).
[37] A. Novick-Cohen, J. Stat. Phys. **38**, 707 (1985).
[38] A. Novick-Cohen, Physica D **26**, 403 (1987).
[39] A. Novick-Cohen and L. A. Peltier, Proc. - R. Soc. Edinburgh, Sect. A: Math. **123**, 1071 (1993).
[40] M. Grinfield and A. Novick-Cohen, Proc. - R. Soc. Edinburgh, Sect. A: Math. **125**, 351 (1995).
[41] J. D. Gunton, M. San Miguel, and P. S. Sanhi, in *Phase Transitions and Critical Phenomena*, edited by D. Domb and J. L. Lebowitz (Academic Press, London, 1983), Vol. 8, pp. 267 and 466.
[42] A. D. Rutemberg and A. J. Bray, Phys. Rev. E **51**, 5499, 1999.
[43] N. Alikakos, P. W. Bates, and G. Fusco, J. Diff. Eqns. **90**, 81 (1991).
[44] M. Abramowitz and I. Stegun, *Handbook of Mathematical Functions* (Dover Publications, New York, 1972).
[45] J. C. Eilbeck, J. E. Furter, and M. Grinfeld, Phys. Lett. A **135**, 272 (1989).
[46] P. W. Bates and P. C. Fife, SIAM J. Appl. Math. **53**, 990 (1993).
[47] H. Calisto, M. Clerc, R. Rojas, and E. Tirapegui, Phys. Rev. Lett. **85**, 3805 (2000).
[48] M. Argentina and M. G. Clerc (unpublished).